J Vis (2010) 13:311–318
DOI 10.1007/s12650-010-0055-9

REGULAR PAPER

Young Il Jang · Sang Joon Lee

POD analysis on the sphere wake at a subcritical Reynolds number

Received: 24 February 2010 / Accepted: 8 September 2010 / Published online: 19 October 2010

Abstract Flow characteristics of turbulent wake behind a sphere at a subcritical flow regime were experimentally investigated. The particle image velocimetry measurements and proper orthogonal decomposition (POD) modal analysis were employed to get detailed flow information such as the wavy structure, swirling motion and coherent structures of the sphere wake. The variation of turbulent intensities of the radial and circumferential velocity components showed the swirling motion of sphere wake in the cross-sectional planes. The relative contribution of the POD mode 1, 2 and 3 in eigenvalues was 26, 11, and 8%, respectively. The general pattern of velocity fields for the POD mode 1 in the near-wake region of $x/d = 0.7$–1.4 is similar with that of time-averaged mean velocity fields. In addition, the sweeping flow in the region from $x/d = 1.5$ to $x/d = 2.0$ possesses wavy structure of the sphere wake. The experimental results of the present study would contribute to the fundamental understanding of the turbulent near-wake behind a sphere.

Keywords Sphere · POD · Turbulent wake · PIV

1 Introduction

Sphere is considered as an idealized model of three-dimensional axisymmetric bluff bodies. Because a sphere is a basic body shape which has a large potential for various applications, many researchers have studied the flow around a sphere (Kim and Durbin 1988; Sakamoto and Haniu 1990; Jang and Lee 2007, 2008). However, due to very limited experimental studies reported, detailed information on the vortical structures behind a sphere at $Re \approx 10^4$ is not available yet. In addition, the wavy structure and swirling motion in cross-sectional planes of near-wake need also to be investigated experimentally to understand the vortical structure of the sphere wake.

Since turbulent flows involve complicated interaction of many degrees of freedom over broad ranges of spatial and temporal scales, the small-scale turbulence is embedded in the large scale and vice versa. Coherent structures are organized features which repeatedly appear and undergo a characteristic temporal cycle (Berkooz et al. 1993). Proper orthogonal decomposition (POD) offers a rational method to extract coherent structure. POD is a modal description for coherent structures and enables us to reconstruct each

Y. I. Jang
Department of Aerospace and Mechanical Engineering, ROK Air Force Academy, Choongbuk 363-840, Korea

S. J. Lee (✉)
Department of Mechanical Engineering, Pohang University of Science and Technology,
San 31, Hyo-Ja Dong, Pohang 790-784, Korea
E-mail: sjlee@postech.ac.kr
Tel.: +82-54-2792169
Fax: +82-54-2793199

dominant instantaneous velocity field. Using POD modal analysis, flow characteristics of the near-wake and turbulent flow over a sphere can be investigated in different point of view, which is difficult to observe in the time-averaged analysis.

In this study, the velocity vector fields in the cross-sectional planes behind a sphere model were obtained using a particle image velocimetry (PIV) technique to get the spatial distributions of in-plane velocities and turbulence statistics in the near-wake. Then, the POD modal characteristics of coherent structure were analyzed by deriving eigenvalues and spatial modes using the snapshot method in the cross-sectional planes. Critical point concepts are employed in the analysis of the modal flow pattern. Through these systematic experiments, we hope to understand the wavy structure, swirling characteristics and coherent structures in the near-wake behind a sphere.

2 Experimental methods

2.1 PIV measurements

The cross-sectional plane behind a sphere was illuminated from the bottom side of the test section as shown in Fig. 1. The y–z cross-sectional plane is the plane orthogonal to the streamwise direction (x). The free stream velocity was fixed at $U_0 = 13$ cm/s at which the turbulent intensity was below 0.28%. The Reynolds number based on the free stream velocity and sphere diameter (d) was $Re = 11{,}000$. Five hundred pairs of PIV particle images were captured at a 4 Hz sampling rate for each experimental condition. The detailed experimental methods were described in Jang and Lee (2008). The orthogonal in-plane velocity components (V_y, V_z) in the y–z plane were extracted at each grid point and these velocity components were decomposed into the radial and circumferential velocity components (V_r, V_θ) in the polar coordinate as shown in Fig. 1b. The spatial resolution of the velocity vector fields was 0.23×0.23 cm^2.

2.2 POD formulation

The mathematical formulation of POD has been well established by several researchers (Holmes et al. 1996; Berkooz et al. 1993; Sirovich 1987). In Reynolds decomposition, an instantaneous velocity can be decomposed into mean velocity and fluctuating velocity component. In POD, the fluctuating velocity component can be expressed as the sum of temporal mode coefficients a_n uncorrelated with time, multiplied by normalized base functions ϕ_n which are spatially orthogonal:

$$u(\vec{x},t) = U(\vec{x}) + u'(\vec{x},t) = U(\vec{x}) + \sum_{n=1}^{N} a_n(t)\phi_n(\vec{x}) \tag{1}$$

Here, N is the total number of modes. To derive a_n and ϕ_n, the base function ϕ is chosen to be maximized in the averaged projection of u onto ϕ,

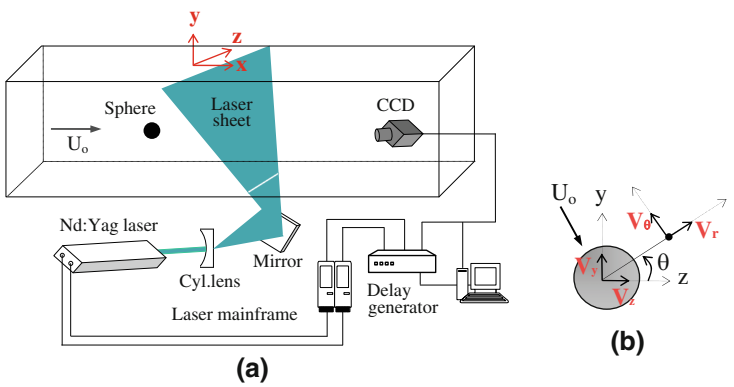

Fig. 1 Schematic diagram of experimental setup and velocity decomposition in the polar coordinate: **a** PIV measurement systems and **b** velocity decomposition

$$\max_{\phi} \frac{\langle |(u,\phi)|^2 \rangle}{||\phi||^2} \tag{2}$$

where (,) denotes the inner product and | | is the modulus. In addition, $\langle \cdot \rangle$ denotes the ensemble average and $||f||$ is the norm, $(f,f)^{1/2}$. The solution of this equation leads to the following eigenvalue problem,

$$\int R(x,x')\phi(x')\,\mathrm{d}x' = \lambda\phi(x) \tag{3}$$

$$R(x,x') = \langle u(x)u(x') \rangle \tag{4}$$

Here, R is the averaged two-point correlation tensor. The maximum in Eq. 2 corresponds to the largest eigenvalue λ_1 of Eq. 3. Moreover, there is not one, but a numerable solutions of Eq. 3. The eigenvalues are ordered by $\lambda_i \geq \lambda_{i+1}$, observing that the non-negative definiteness of Eq. 4 assures that $\lambda_i \geq 0$. If the number of vector is N, R becomes $N \times N$ matrix in the direct method of POD and hence the dimension of R is rapidly increased with the number of vector. Therefore, it takes too much computation to obtain R. This time-consuming problem can be resolved to $M \times M$ matrix calculation by employing the method of snapshots proposed by Sirovich (1987). Here, M is the number of ensembles and usually M is smaller than N in PIV experiments. The underlying mathematical assumptions and their validation are the same between two methods of POD. In the snapshot method, Eq. 4 is replaced by a following degenerate kernel,

$$\mathbf{C} = \frac{1}{M}\sum_{k=1}^{M} (\mathbf{u}(t_i), \mathbf{u}(t_k)) \tag{5}$$

where $\mathbf{C}$ is $M \times M$ two-point correlation matrix (bold character means matrix) and the eigenfunction ϕ can be expressed as follows,

$$\phi = \sum_{k=1}^{M} a_k \mathbf{u}^k \tag{6}$$

Here, the temporal mode coefficients a_k remain to be determined. The M-dimensional eigenfunction problem can finally be written as,

$$\sum_{k=1}^{M} \frac{1}{M} (\mathbf{u}(t_i), \mathbf{u}(t_k)) a_k = \lambda a_i; \quad i = 1, \ldots, M \tag{7}$$

The solution of Eq. 7 results in M-ordered eigenvalues and corresponding M eigenvectors. If $\mathbf{u}$ is a turbulent velocity field, then the eigenvalues λ_j imply twice the average turbulent kinetic energy at each mode ϕ_j.

In this study, the number of velocity vectors was $N = 4{,}096$ and the number of ensemble was $M = 500$. The method of snapshots was employed to calculate eigenvalues, temporal mode coefficients and spatial modes for both V_z and V_y velocity components measured in cross-sectional planes of the sphere wake.

3 Results and discussion

3.1 PIV analysis of time-averaged turbulent statistics

Figure 2 shows the spatial distribution of the turbulence intensity of the radial velocity component (V_r). The contours of similar magnitude are distributed in a disk shape at each x/d location. At $x/d = 0.8$ ($x/d = 0.5$ is the aft-end of the sphere model in x-direction), just behind the sphere model, the radial turbulence intensity has relatively larger values circumferentially around the sphere. Its magnitude becomes stronger, and the location of the local maximum values moves from the sphere periphery to the wake center as the flow goes downstream. It has the maximum value at $x/d = 1.2$. This maximum location seems to be interconnected with the onset of shear layer instability (Jang and Lee 2008).

In the downstream region from $x/d = 1.2$ to 1.6, a dipole-shaped region of large turbulence intensity values is centered at the origin and aligned vertically. The main axis of the dipole-shaped region is slightly tilted toward the clockwise direction with going downstream.

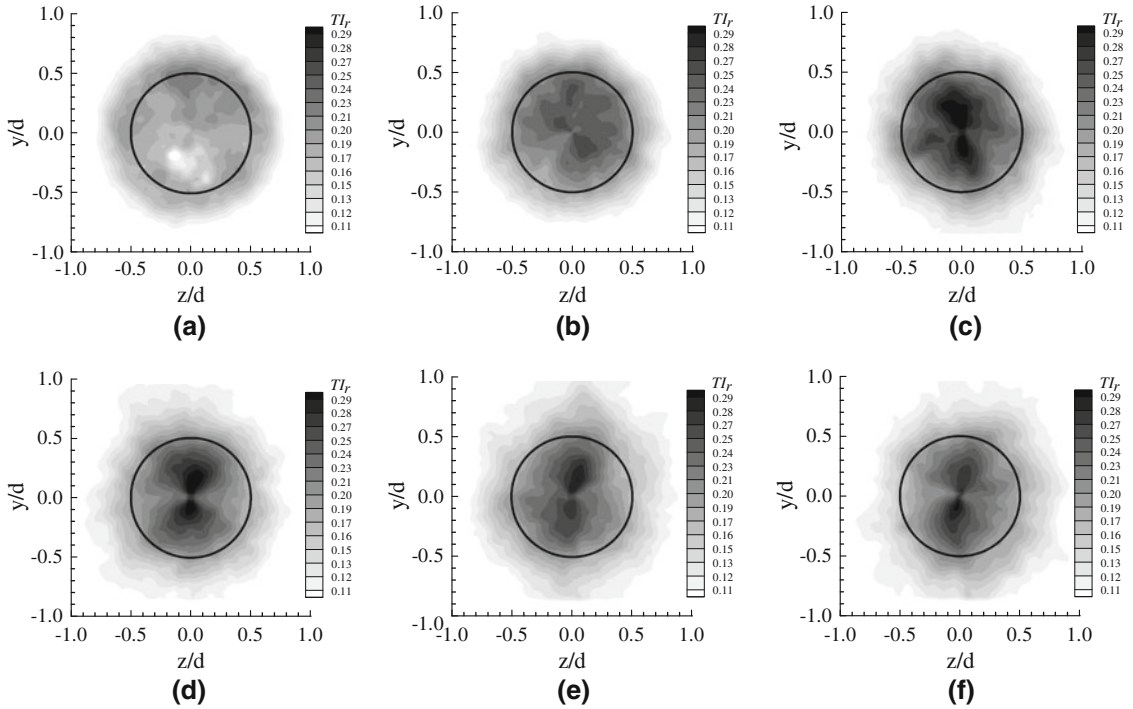

Fig. 2 Spatial distribution of turbulent intensity $\left(\sqrt{\overline{V_r'^2}}\Big/ U_0\,(\%)\right)$: **a** $x/d = 0.8$, **b** $x/d = 1.0$, **c** $x/d = 1.2$, **d** $x/d = 1.4$, **e** $x/d = 1.5$, and **f** $x/d = 1.6$

The spatial distribution of the turbulence intensity of the circumferential velocity component (V_θ) is shown in Fig. 3. The general flow pattern and downstream evolution are similar to those of radial turbulence intensity shown in Fig. 2, excepting the tilted direction of the dipole-shaped region of large values. Unlike the radial turbulence intensity case, the dipole-shaped region centered at the origin is aligned horizontally in the downstream region beyond $x/d = 1.2$. The main axis is slightly tilted clockwise as the flow goes downstream. The results shown in Figs. 2 and 3 also indicate the swirling motion of wake in the downstream region beyond the vortex formation region. This implies that the wake rotates at different speeds in each cross-sectional plane with going downstream. The rotation of wake in the cross-sectional planes has been mentioned in several flow visualization studies (Achebach 1972; Taneda 1978; Sakamoto and Haniu 1990). In addition, Yun et al. (2006) elucidated this feature numerically in detail. These unique patterns of turbulent statistics reflect the wavy or helical turbulent structure of the wake in the cross-sectional planes behind the vortex formation region. Although the turbulent statistics of wavy wake structure in the streamwise plane have been investigated by several researchers (Sakamoto and Haniu 1990; Leder and Geropp 1993; Yun et al. 2006), the helical structure of the sphere wake and its evolution in the cross-sectional planes have not been clearly described yet. The present PIV results of turbulent statistics in the cross-sectional planes are helpful to elucidate the ambiguity of helical structure and the evolution of the sphere wake.

3.2 POD modal characteristics of eigenvalues

Figure 4a shows the convergence of the normalized eigenvalues λ_i. The accumulated sum of eigenvalues ($\Sigma(\lambda_i)$), normalized by the total sum of eigenvalues, reaches 0.99 at this mode 201. The general trend of convergence of the normalized eigenvalues looks similar with those of previous studies on a flow over an elliptic cylinder (Daichin and Lee 2004) or a confined impinging jet (Kim et al. 2007). In their studies, the normalized eigenvalues were converged more rapidly, indicating that a few fore eigenvalues had relatively large portions.

Figure 4b shows the relative contribution of the fore 20 eigenvalues. The fractional portions for λ_1, λ_2 and λ_3 are 26, 11 and 8%, respectively. The lower modes of $\lambda_4 \sim \lambda_6$ have fractional values in the range of 3–5%. The relative contribution of the other remaining eigenvalues is very weak, less than 3%. In the studies of Jung et al. (2004) for a turbulent axisymmetric jet and Oudheusden et al. (2005) for a flow over a square

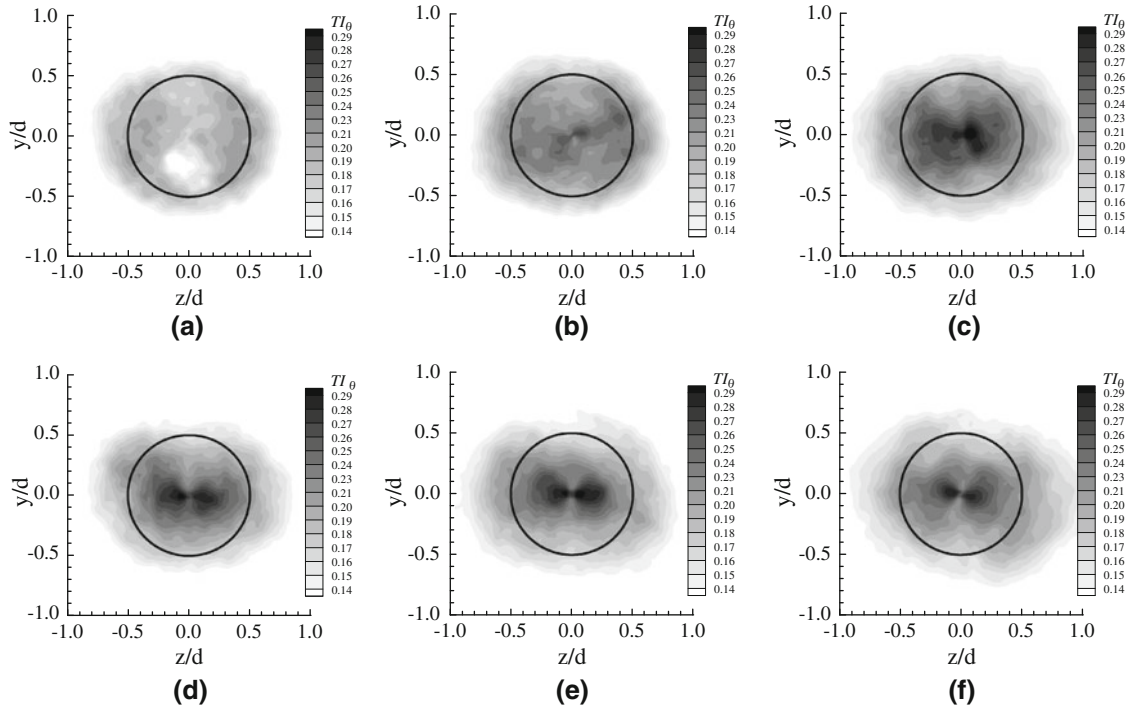

Fig. 3 Spatial distribution of turbulent intensity $\left(\sqrt{\overline{V_\theta'^2}}\Big/ U_0\,(\%)\right)$: **a** $x/d = 0.8$, **b** $x/d = 1.0$, **c** $x/d = 1.2$, **d** $x/d = 1.3$, **e** $x/d = 1.4$, and **f** $x/d = 1.6$

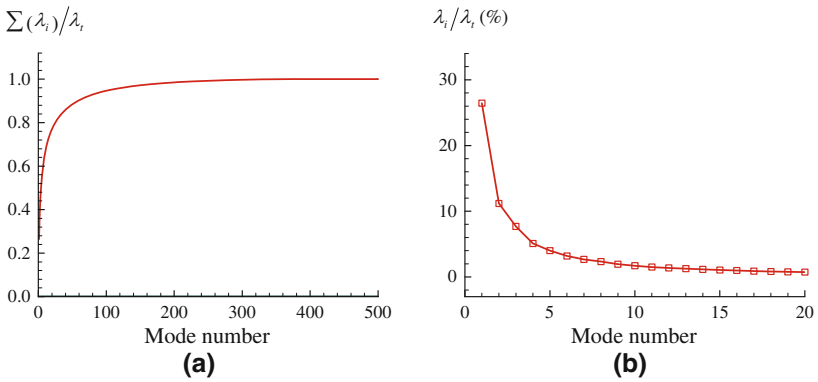

Fig. 4 Convergence and relative contribution of eigenvalues: **a** convergence of normalized eigenvalues and **b** relative contribution of the fore 20 eigenvalues

cylinder, the fore two modes contained more than 60% of the total turbulent kinetic energy. Differently from their works, the fore two modes in the present study contain about 37% of the total turbulent kinetic energy. This implies that the coherent structure of sphere wake is not so strong, compared to an axisymmetric jet and a 2D cylinder wake. This variation of eigenvalues indicates the complicated flow structure of the sphere wake at a subcritical flow regime. As pointed out by Jang and Lee (2007, 2008), the sphere wake at the subcritical flow regime exhibits very complex three-dimensional turbulent flow characteristics. Therefore, the fore POD mode 1 or 2 of the sphere wake does not solely contain large portion of the total turbulent kinetic energy.

3.3 POD modal characteristics of sphere wake

Figure 5 shows the velocity vector fields of POD mode 1 in the cross-sectional planes at various x/d locations. The velocity fields of POD mode 1 at the near-wake region of $x/d = 0.9$–1.4 show similar flow pattern

with the time-averaged velocity fields of Jang and Lee (2008) at corresponding x/d locations. This flow characteristic seems to be attributed to the fact that the POD mode 1 corresponds to the largest value of eigenvalue λ_1. However, the velocity vector fields in the region beyond the location of $x/d = 1.5$ show different flow pattern from the time-averaged velocity fields. At $x/d = 1.5$, the large-scale flow sweeps to downward and left direction, as shown in Fig. 5d. On the other hand, at $x/d = 1.6$ (not shown), the sweeping direction of the wake flow changes to downward and right way. With going downstream, e.g., at $x/d = 1.7$ in Fig. 5e, the sweeping motion changes the flow direction to upward and left side, thereafter, the sweeping flow shifts to upward and right direction at $x/d = 1.8$ (not shown). The sweeping flow goes downward and right direction again at $x/d = 1.9$ in Fig. 5f, while it goes toward the downward and left direction at $x/d = 2.0$. This swirling motion of sweeping flow in the cross-sectional planes from $x/d = 1.5$ to $x/d = 2.0$ indicates the wavy structure of the sphere wake. Because the instantaneous vorticity distributions contain the wavy flow structure of the sphere wake as a function of time at a fixed x/d location in Jang and Lee (2008), the velocity fields of POD mode 1 in Fig. 5 exhibit the wavy pattern in the sphere wake at sequential x/d locations. This points out that the wavy pattern is the dominant coherent structure of the sphere wake.

To describe the flow pattern for POD modes 2–3, the critical point concepts were employed in this study. According to Perry and Chong (1987), the critical points are the locations in the flow where the streamline slope is indeterminate and velocity is zero relative to an appropriate observer. Figure 6 shows the velocity vector fields of POD mode 2 in the cross-sectional planes at three downstream locations. The critical points observed are marked as 'F(foci)' and 'S(saddle)' in the figures. The conspicuous foci and saddle points appear at each x/d location.

Figure 7 shows the velocity vector fields of POD mode 3 at three x/d locations. The number of critical points is increased, compared to that of the POD mode 2. In addition, new 'N(node)' points are observed at a few x/d locations. Moreover, the paired foci and saddle points are frequently appeared in POD mode 3. This kind of unique distribution patterns of critical points including the large-scale circulatory vortex in the POD spatial modes has not been observed in the instantaneous and time-averaged mean velocity fields of Jang and Lee (2008). Figures 5, 6 and 7 demonstrate the usefulness of POD decomposition in the identification of obscured coherent structures.

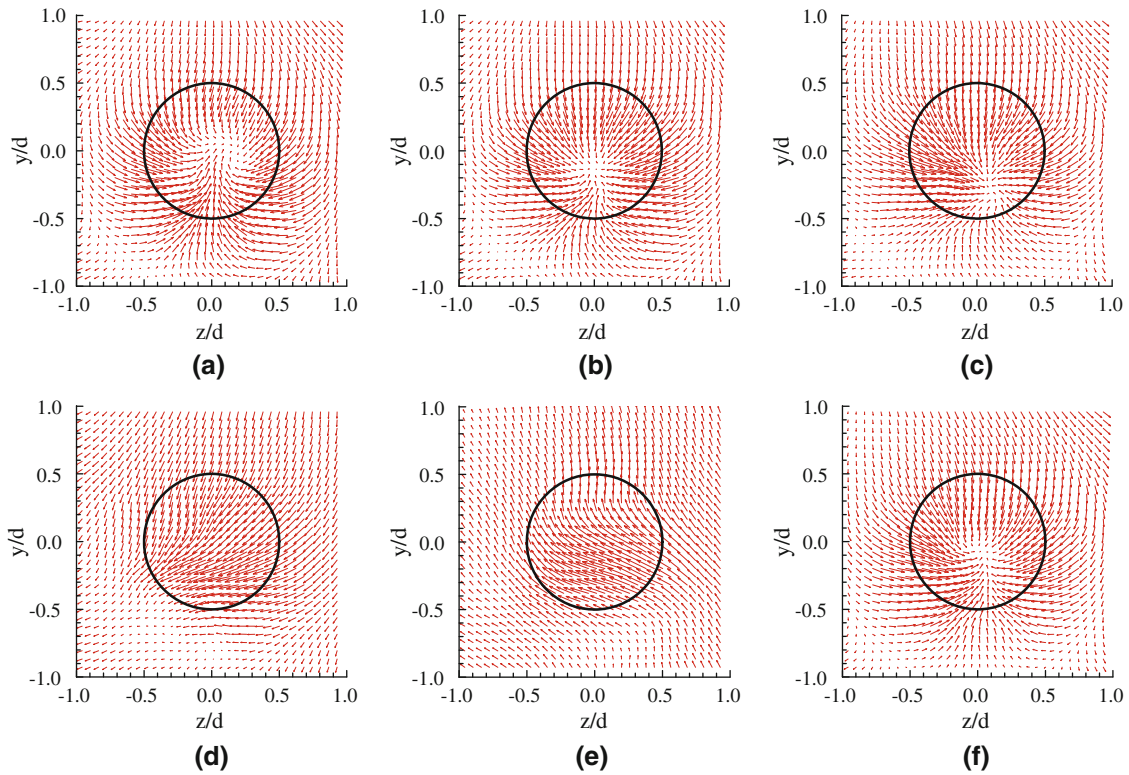

Fig. 5 Velocity vector fields of POD mode 1 at various x/d locations: **a** $x/d = 0.9$, **b** $x/d = 1.1$, **c** $x/d = 1.3$, **d** $x/d = 1.5$, **e** $x/d = 1.7$, and **f** $x/d = 1.9$

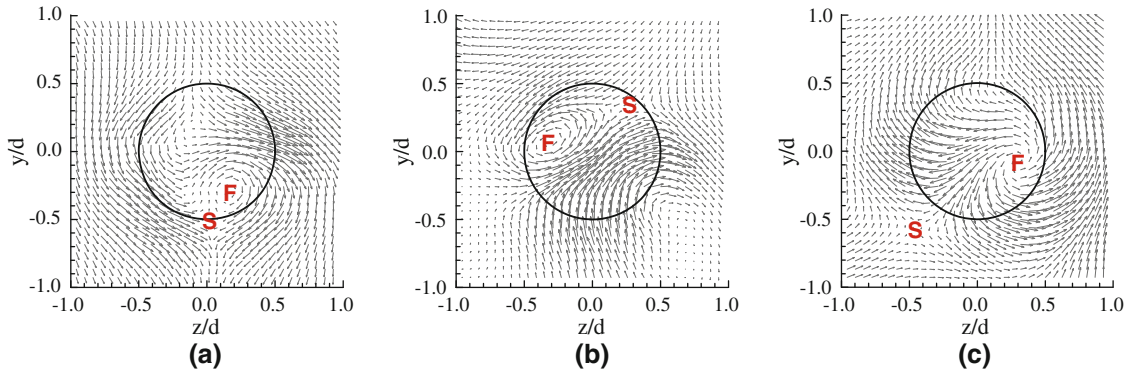

Fig. 6 Velocity vector fields of POD mode 2 at various x/d locations: **a** $x/d = 0.8$, **b** $x/d = 0.9$, and **c** $x/d = 1.7$

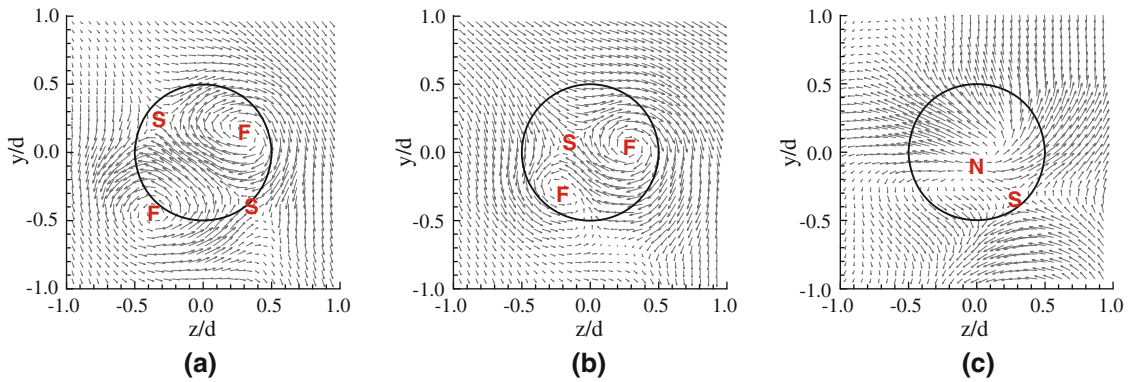

Fig. 7 Velocity vector fields of POD mode 3 at various x/d locations: **a** $x/d = 0.8$, **b** $x/d = 1.5$, and **c** $x/d = 1.7$

4 Conclusions

The flow characteristics of turbulent wake behind a sphere at a Reynolds number of $Re = 11{,}000$ were experimentally investigated. The detailed flow information such as wavy structure, swirling motion and coherent structures of the sphere wake at a subcritical flow regime was explained using the quantitative experimental results obtained from PIV measurements and POD modal analysis. The POD modal characteristics of coherent structure were analyzed to extract eigenvalues and spatial modes by applying the snapshot method to the velocity field measured at several cross-sectional planes of the sphere wake.

The variation of turbulence intensities of the radial and circumferential velocity components shows the swirling motion of sphere wake in the cross-sectional planes which elucidates the wavy or helical turbulent structure of the sphere wake. In the POD modal analysis, the relative contributions of the POD modes 1, 2 and 3 in eigenvalues are 26, 11, and 8%, respectively. The general flow pattern of the velocity fields of POD mode 1 in the region of $x/d = 0.9$–1.4 is similar with that of the time-averaged velocity fields. On the other hand, the sphere wake in the region from $x/d = 1.5$ to $x/d = 1.9$ shows the directional variation of flow pattern at downstream locations, indicating that the wavy pattern is a predominant coherent structure of the sphere wake.

The present experimental results on the sphere near-wake would contribute to the fundamental understanding of the turbulent wake behind a sphere and provide useful data in validating numerical predictions at a subcritical flow regime.

Acknowledgments This work was supported by Creative Research Initiatives (Diagnosis of Biofluid Flow Phenomena and Biomimic Research) of MEST/KOSEF.

References

Achebach E (1972) Experiments on the flow past spheres at very high Reynolds numbers. J Fluid Mech 54:565–575
Berkooz G, Holmes P, Lumley JL (1993) The proper orthogonal decomposition in the analysis of turbulent flows. Annu Rev Fluid Mech 25:539–575
Daichin, Lee SJ (2004) POD analysis of near-wake structures of an elliptic cylinder adjacent to a free surface. J Vis 7:179–186
Holmes P, Lumley JL, Berkooz G (1996) Turbulence, coherent structures, dynamical systems and symmetry. Cambridge University Press, Cambridge
Jang YI, Lee SJ (2007) Visualization of turbulent flow around a sphere at subcritical Reynolds numbers. J Vis 10:359–366
Jang YI, Lee SJ (2008) PIV analysis of near-wake behind a sphere at a subcritical Reynolds number. Exp Fluids 44:905–914
Jung D, Gamard S, George WK (2004) Downstream evolution of the most energetic modes in a turbulent axisymmetric jet at high Reynolds number. Part 1. The near-field region. J Fluid Mech 514:173–204
Kim HJ, Durbin PA (1988) Observations of the frequencies in a sphere wake and of drag increase by acoustic excitation. Phys Fluids 31:3260–3265
Kim KC, Min YU, Oh SJ, An NH, Seoudi B, Chun HH, Lee I (2007) Time-resolved PIV investigation on the unsteadiness of a low Reynolds number confined impinging jet. J Vis 10:367–379
Leder A, Geropp D (1993) The unsteady flow structure in the wake of the sphere. SPIE 2052:119–126
Oudheusden BW, Scarano F, Hinsberg NP, Watt DW (2005) Phase-resolved characterization of vortex shedding in the near wake of a square-section cylinder at incidence. Exp Fluids 39:86–98
Perry AE, Chong MS (1987) A description of eddying motions and flow patterns using critical-points concepts. Annu Rev Fluid Mech 19:125–155
Sakamoto H, Haniu H (1990) A study on vortex shedding from spheres in a uniform flow. J Fluids Eng 112:386–392
Sirovich L (1987) Turbulence and the dynamics of coherent structures. Q Appl Math 45:561–590
Taneda S (1978) Visual observations of the flow past a sphere at Reynolds numbers between 10^4 and 10^6. J Fluid Mech 85:187–192
Yun G, Kim D, Choi H (2006) Vortical structures behind a sphere at subcritical Reynolds numbers. Phys Fluids 18:015102